Aerothermodynamic Analysis and High-Speed Schlieren Imaging of an Undergraduate-Designed Hypersonic Glide Vehicle

Aaron K. Matheny* and Isaac S. Smith†
University of Tennessee, Knoxville, Tennessee, 37996, USA

This paper details the aerothermodynamic analysis and subsequent wind tunnel validation of Tachyon, an unpowered, highly maneuverable, hypersonic glide vehicle for low-altitude operation designed by the Student Space Technology Association (SSTA) for an undergraduate competition hosted by the University Consortium for Applied Hypersonics (UCAH) in conjunction with the Joint Hypersonics Transition Office (JHTO). This design was ultimately selected as one of three winners nationwide, in large part due to the quality and depth of the data collection methodology detailed in this paper. The extreme aerothermodynamic environment characteristic of hypersonic flight necessitates the use of advanced computational tools capable of modeling high-temperature gas dynamics. NASA's Configuration-Based AERОdynamics (CBAERO) is a panel method code that assesses the aerothermodynamic characteristics of an unstructured surface mesh. CBAERO is computationally inexpensive relative to Computational Fluid Dynamics (CFD) and thus is suited for rapid preliminary analysis. For more robust analysis, NASA's Fully UNstructured 3D (FUN3D), a CFD code capable of modeling high-temperature gas effects, is utilized. Both tools are validated against each other and against results from Mach 7 wind tunnel testing performed at the University of Tennessee Space Institute (UTSI) using a one-third scale model of Tachyon. Experimental data using infrared thermal imaging and high-speed schlieren imaging are collected and compared to CFD heating and shock formation results to validate the simulations run at wind tunnel conditions. The error between the CFD and wind tunnel heat flux values were calculated at stations in key areas of the vehicle. From this analysis, each surface was assigned a heating correction factor which was then used to determine convection boundary conditions (BC's) based on CFD results for heat transfer finite element analysis (FEA). The several data collection methods employed demonstrated strong agreement in shockwave patterns and surface heating distributions, though substantial discrepancies emerged in the magnitude of the heating numbers on the bottom surface of the vehicle.

I. Introduction

The design and analysis of hypersonic systems is increasingly relevant to modern aeronautical science, particularly with respect to national defense [1, 2]. The capabilities of hypersonic systems have expanded in the current day, and new hypersonic configurations such as boost-glide systems, cruise missiles, interceptors, reusable aircraft, and gun-launched projectiles have all become subjects of extensive development and exploration due to their implications in national defense [3–5]. To address the rising prevalence of hypersonics, the United States Department of Defense (DoD) founded the Joint Hypersonics Transition Office (JHTO), a DoD agency with the objective of furthering hypersonic technology research, devlopment, and workforce capability [6]. A primary achievement of JHTO was the creation of the University Consortium for Applied Hypersonics (UCAH), a university network dedicated to furthering university research in areas critical to the advancement of hypersonics as well as stimulating workforce development at the graduate and undergraduate level [6, 7]. Most notably, UCAH recently hosted the 2025 Undergraduate Hypersonic Flight Design Competition, a national undergraduate design competition with more than 30 university participants [8]. The objective of the competition was to design an unpowered, high lift-to-drag, hypersonic projectile utilizing modern simulation and design tools to validate the aerodynamic efficacy and thermal survivability of the design [8].

Ground testing and computational analysis of hypersonic systems remains a challenging area drawing significant research investment. The physical complexity of the flow regime necessitates highly interdisciplinary research spanning fields such as aerodynamics, thermodynamics, chemistry, scientific computing, and materials science [2]. The high stagnation enthalpy and extreme viscous dissipation characteristic of high Mach number flows result in extremely

*Undergraduate Student, Mechanical and Aerospace Engineering, Student Member, 1810514
†Undergraduate Student, Mechanical and Aerospace Engineering, Student Member, 1924459

high temperatures within the shock layer and boundary layers of a hypersonic vehicle [9, 10], which emphasizes the importance of aerothermal analysis to validate the thermal survivability of a selected design under extreme heat loads [11–13]. However, these high temperatures can induce chemical reactions within the flow [9, 10], and modeling these chemical reactions is necessary to obtain accurate results for surface heating and aerodynamic coefficients [10]. The most cost-effective approximation of these important parameters is provided by a numerical solution from performing Computational Fluid Dynamics (CFD) [10], but numerical solutions to chemically reacting flowfields are incredibly complex and computationally expensive [14–16]. Additionally, due to the prohibitive computational expense of a direct numerical solution (DNS) to resolve turbulence [17] and the lower but still large computational expense of large eddy simulation (LES) [14], most hypersonic CFD workflows in industry utilize Reynolds-Averaged Navier-Stokes (RANS) turbulence modeling [18]. RANS enables hypersonic CFD simulations to be run within a practical time span, but has significant uncertainty in the prediction of surface heating [18–20]. Thus, an important aspect of the design and analysis process for hypersonic vehicles is validation of numerical results through ground testing and flight testing.

To meet the design mission set out by UCAH, the Student Space Technology Association (SSTA), an undergraduate rocketry and aerospace technology club based at the University of Tennessee, Knoxville (UTK), developed Tachyon, a hypersonic wedge-derived lifting body designed for the Mach 5-8 flight regime at low altitude. The competition required the design to be thermally survivable, structurally sound, highly maneuverable, and subject to sizing constraints while maximizing range and affordability [8]. The shaping of Tachyon's final geometry was driven by the analysis detailed in this paper in an iterative design process. The selected design was deemed optimal within the parameters of the competition, as evaluated by the analysis performed. Out of the pool of competing teams, Tachyon was selected as one of three winners nationwide [21], and will receive funding from UCAH for a ground test campaign by CUBRC in the 48-inch Large Energy National Shock (LENS) Tunnel [22] and a flight test by the Army Research Laboratory (ARL) [23]. The SSTA's victory in this competition was greatly aided by the rigor of the data collection methodology discussed in this paper, which was comprised of preliminary analysis with the NASA panel method code Configuration Based AEROdynammics (CBAERO) [24], RANS CFD with NASA's Fully UNstructured 3D (FUN3D) [25], and a ground test campaign in the Mach 7 HORIZON Ludwieg Tube at the University of Tennessee Space Institute (UTSI) [26]. Results from this analysis were used to inform the viability of preliminary designs, build an aerodynamic database for trajectory generation, assess the surface heating and thermal survivability of the vehicle, and validate the structural integrity of the fins when subject to high g-loading.

II. Methodology

A. Goals of Analysis

The Request For Proposal (RFP) of the competition called for a long-range, thermally survivable glide vehicle with an insulated interior. Trajectory analysis was required to demonstrate the maximum range of the vehicle within the constraints of a 9 km altitude ceiling and impact velocity of Mach 2. The thermal survivability of all vehicle components from launch to impact was required to be demonstrated. The internal payload section of the vehicle was also required to be thermally protected such that the internal temperature at final impact did not exceed 74 °C.

From these requirements, the ultimate goals of analysis were to generate a trajectory, demonstrate thermal survivability, and verify the efficacy of Tachyon's thermal protection system (TPS). The trajectory generation process itself is not within the scope of the paper, but the trajectory software utilized required an aerodynamic database containing lift, drag, and moment coefficients across a wide range of flight conditions. The thermal requirements were planned to be verified through transient heat transfer finite element analysis (FEA) using convection boundary conditions (BC's) derived from CFD heating numbers.

CBAERO was utilized early in the design process for rapid aerodynamic analysis. The low computational cost of CBAERO allowed the Tachyon design team to rapidly filter through the design space, accelerating development of an optimized geometry. Once a final geometry was selected based on CBAERO results, RANS CFD was run with FUN3D to assess the surface heating and create an aerodynamic database. To validate CFD heating results and shock formation, a week-long ground test campaign was conducted in the University of Tennessee Space Institute (UTSI) Mach 7 Ludwieg tube with data collected from Infrared (IR) cameras and high-speed schlieren imaging. These data were reduced and compared to CFD results as shown in section III.B.

B. Geometry and Flow Conditions

The external geometry of Tachyon used in the CFD analysis was dimensioned as shown in Fig. 1. Tachyon is a wedge-derived lifting body with a six-fin arrangement, flat top parallel to the freestream, and a tapered tail. The point of zero angle of attack is defined with the top parallel to the freestream.

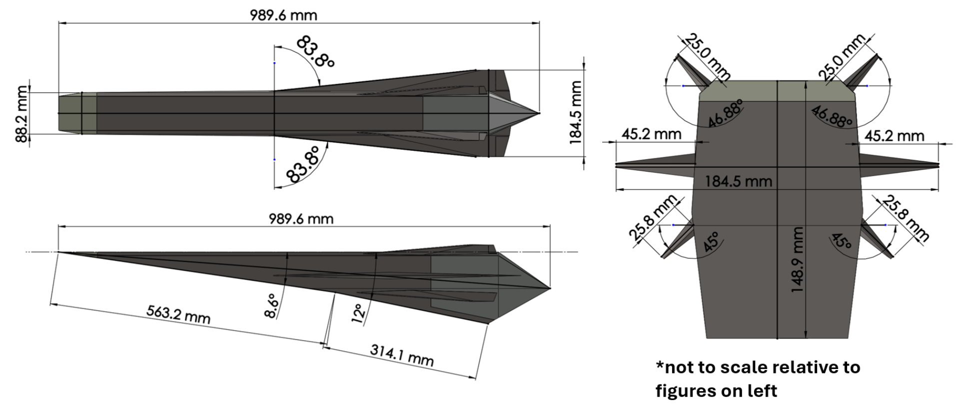

Fig. 1 Top, side, and front views of Tachyon with key dimensions

Flow conditions for CBAERO were based on early estimates of Tachyon's trajectory, and the geometry was shaped around these results. After finalizing an external geometry, FUN3D was utilized to construct an aerodynamic database at the flight conditions shown in Table 1. Upon the completion of the final aerodynamic database, a more accurate trajectory was generated. To reduce the number of FUN3D cases required, key aerothermodynamic environments of interest for heating were determined based on Tachyon's final trajectory generated based on the FUN3D aerodynamic database. The defining parameters for aerodynamic heating analyses are the freestream Mach number and altitude above sea level.

Figure 3 shows the most time Tachyon spends in different aerothermodynamic environments and was used to determine the flow conditions at which heating numbers were desired for FEA. Tachyon is launched at sea level at Mach 8 and decelerates to below Mach 6 at an altitude of 7 km within 10 seconds. Then, Tachyon cruises near the 9 km altitude ceiling for an additional 40 seconds and begins its descent at just over Mach 3, making final impact at Mach 2 around 20 seconds later. Based on the trajectory and the desire for a conservative estimate, flow conditions for transient FEA were determined as summarized in Table 2 and visualized in Fig. 3. To closely model the actual flight path, the plan for FEA analysis was to initialize at 293 K, and then run the BC's in sequence for a specified time, restarting from the previous case's solution field.

Table 1 Case matrix for CFD aerodynamic database

M_∞	α	β
2.0, 4.0, 6.0, 7.0, 8.0	-5.0, 0.0, 2.5, 5.0, 10.0	0.0, 5.0

Table 2 Flow conditions for heating analysis

M_∞	Altitude (km)	Duration (s)
8.0	0.0	10.0
7.0	9.0	40.0
4.0	0.0	20.0

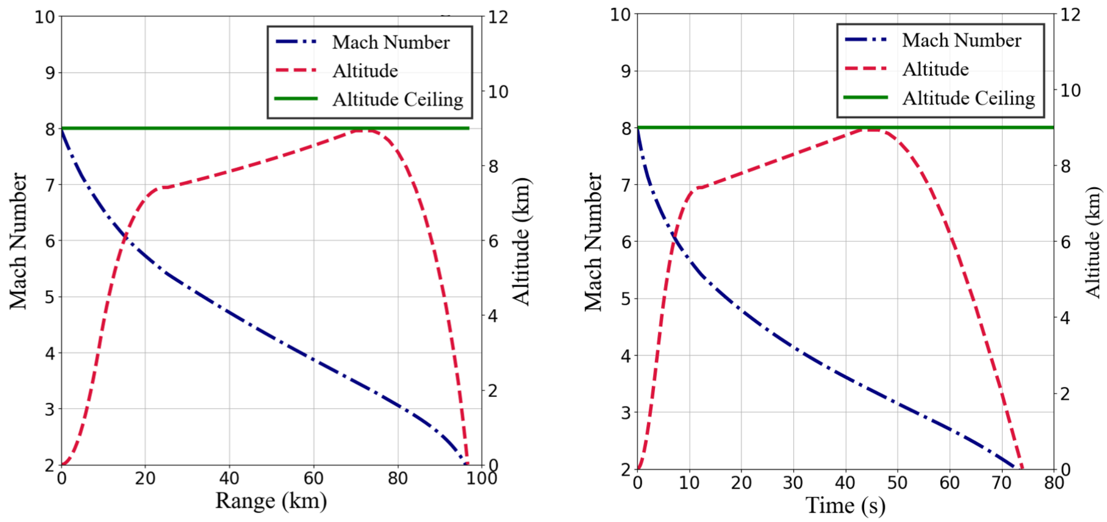

Fig. 2 Final trajectory of Tachyon, calculate based on aerodynamic coefficients from aerodynamic database generated by results from FUN3D

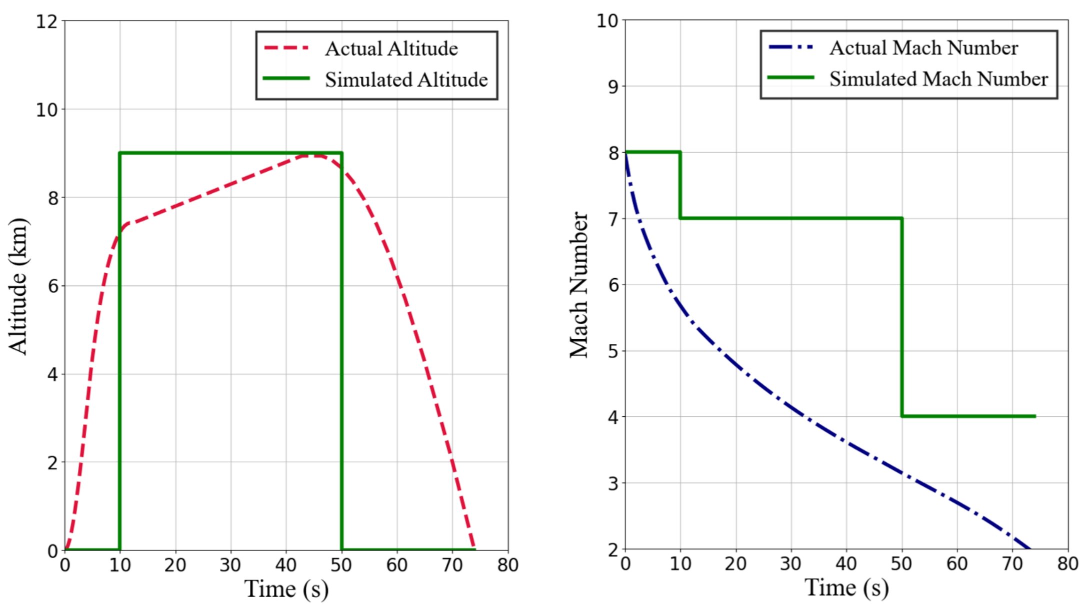

Fig. 3 Simulated flow conditions compared to actual flight conditions

SolidWorks Simulation was employed for time-accurate FEA. Convection BC's in SolidWorks require a convection coefficient $\bar{h}$ and fluid temperature T. To obtain these parameters from FUN3D, both isothermal and adiabatic cases were run at the flow conditions given in Table 2. The wall heat flux $q_w^{''}$ was obtained from an isothermal case with a specified wall temperature $T_{w,\mathrm{iso}}$. The temperature used to define the convection BC for FEA, taken to be equal to the adiabatic wall temperature $T_{w,\mathrm{ad}}$, was obtained from an adiabatic case. Convection coefficient was found as shown in Eq. (1).

$$\bar{h} = \frac{q_w^{''}}{T_{w,\mathrm{iso}} - T_{w,\mathrm{ad}}} \quad \text{(Ref.[13])} \tag{1}$$

C. CFD Procedure

Steady-state RANS CFD was performed with FUN3D v.13.7. Cases above Mach 4 were run with FUN3D's generic gas equation set with a one-temperature, five-species air, finite-rate reacting gas model with the governing equations given in chapter 2 of [25]. Cases below Mach 4 were run with FUN3D's compressible equation set given in chapter 2 of [25] with a calorically perfect gas model. The one-temperature cases were run with Wilcox's k-ω turbulence model [27] and Yee's symmetric total variation diminishing inviscid flux scheme [28] with a minmod limiter. Calorically perfect cases were run with Menter's baseline two-equation model [29] and van Leer's inviscid flux scheme [30] with the van Albada limiter [31]. The computational domain was defined with a farfield BC on the outer surfaces of the mesh, a symmetry BC for the centerline plane, and a no-slip wall BC for the external surfaces of Tachyon. For cases where only aerodynamic data were desired, walls were modeled as adiabatic. Isothermal wall BC's were prescribed only where heating data were desired. Input parameters for each case are summarized in Table 3 in accordance with the flow conditions in Tables 1 and 2.

Table 3 Summary of FUN3D inputs for all cases

Case	Chemical Kinetics	Thermal Model	M_∞	Re_∞(1/m)	T_∞(K)	T_w(K)	Turbulence
M8 Aero	Finite Rate	1T	8.0	7.6x10^7	229.7	Adiabatic	Wilcox k-ω (2006)
M7 Aero	Finite Rate	1T	7.0	6.7x10^7	229.7	Adiabatic	Wilcox k-ω (2006)
M6 Aero	Finite Rate	1T	6.0	5.7x10^7	229.7	Adiabatic	Wilcox k-ω (2006)
M4 Aero	N/A	CPG	4.0	3.8x10^7	229.7	Adiabatic	Menter Baseline
M2 Aero	N/A	CPG	2.0	1.9x10^7	229.7	Adiabatic	Menter Baseline
M8 Heating	Finite Rate	1T	8.0	19x10^7	288.15	Adiabatic OR 288.15	Wilcox k-ω (2006)
M7 Heating	Finite Rate	1T	7.0	6.7x10^7	229.7	Adiabatic OR 288.15	Wilcox k-ω (2006)
M4 Heating	N/A	CPG	4.0	9.3x10^7	288.15	Adiabatic OR 288.15	Menter Baseline

All cases were run with FUN3D's steady-state solver. The Courant–Friedrichs–Lewy (CFL) number was ramped to accelerate convergence. The ramping iterations and bounds were manually adjusted for each case whenever stability issues arose, though the CFL number was never raised greater than 10. For each case, a certain number of first order iterations were prescribed to aid stability before the flow field had developed. The number of first order iterations was different for each case, with the more extreme cases typically given around 1000 and the more stable cases given around 300. Convergence was assessed based on the L_2 residual norms dropping at least 5 orders of magnitude and approaching steady values. Additionally, the C_L,C_D, and C_{My} were monitored, with a case being deemed sufficiently converged if these parameters fluctuated by no more than 0.1% over a window spanning 250 iterations. For the cases where heating data were sought, convergence was additionally assessed by q'' sampled at several points along Tachyon's surface, with fluctuation of no more than 1.0% over a window spanning 500 iterations being deemed sufficient.

Most of these cases were run with a 12 million cell semi-span symmetric mesh. The half-symmetry assumption was validated by running a full, non-symmetric mesh and comparing the values of C_L and C_D from a case run with a Mach 7, altitude 9 km flow condition. The C_L and C_D from a half-symmetry and a full geometry case were within 3% of each other, so the half-symmetry simplification was deemed appropriate. Sideslip cases were run with the full, 24 million cell mesh.

Mesh generation was performed with Fidelity Pointwise v.2024.2.3. An unstructured mesh was created with viscous refinement generated by the T-Rex algorithm with a growth rate of 1.2 and initial wall height of 1.00 μm as shown in Fig. 4. A y^+ value below 0.10 was desired to sufficiently resolve heating. The *a posteriori* average y^+ of 0.005 was calculated with a maximum of 0.31. FUN3D jobs were run utilizing High Performance Computing (HPC) resources on the University of Tennessee's Infrastructure for Scientific Applications and Advanced Computing (ISAAC) Secure Enclave cluster. Each job was run on 2 nodes with 96 CPU cores each, with each case taking around 24-48 hours wall clock time to converge.

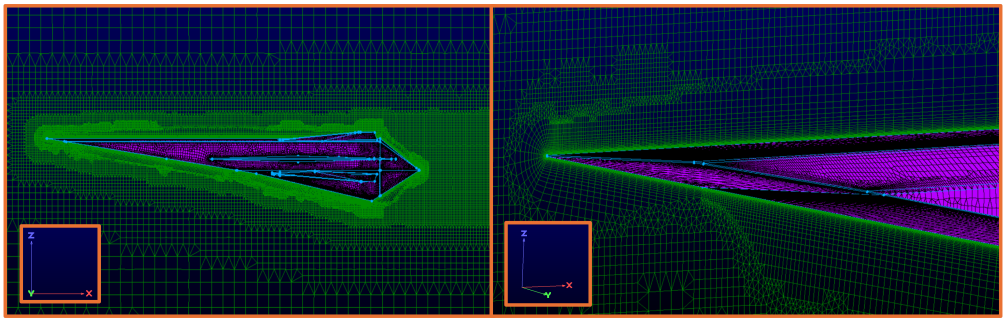

Fig. 4 Pointwise-generated mesh showing buttline center-line slice and surface mesh (left) and enhanced view of mesh refinement in the stagnation region (right)

D. UTSI Wind Tunnel Testing

A 1:3 scale model of Tachyon was tested in the HORIZON Research Group Mach 7 Ludwieg tube wind tunnel facility at UTSI. This facility has the capability to run high-frequency infrared and schlieren imaging diagnostics. The Ludwieg tube has a variable nominal stagnation pressure and temperature, with a useful flow duration of approximately 100 ms [32].

The Tachyon model was tested at a nominal driver pressure of 6.89 kPa and a temperature of 561 K, providing a flow density of 0.022 $\frac{kg}{m^3}$ equivalent to 27 km altitude in the test section with a Reynolds number per unit length of 5.1×10^6 $\frac{1}{m}$. The test section flow speed is measured at 1049 m/s during the second wave passage period [26]. All heating measurements were taken during the second wave passage period, when the flow is the most stable and conducive to accurate measurements. The test model was 3D printed at 1/3 scale out of polylactic acid (PLA) plastic material and treated with acetone to reduce surface roughness. The test model was then mounted on a stainless steel sting in the test section, where its vertical and horizontal angles could be adjusted to imitate pitch and sideslip conditions in the laminar flow of the test section.

A FLIR X8581 IR camera was pointed downwards from the top of the test section at the model, and a high-speed camera with Z-type schlieren setup was angled through the side of the test section. For test runs, the model was oriented either upright or inverted in the test section, allowing for upper and lower surface IR measurements and side-viewing schlieren imagery. IR camera data were captured at 200 Hz while schlieren imagery was captured at 5000 Hz.

Testing conducted over the span of a week at UTSI allowed for the creation of a database documenting performance of the model at different angles of attack and sideslip to, matching some of the values in Table 1. IR camera data provided temperature changes over the flow duration, which were used to calculate predicted heating values. Schlieren imagery was used to validate calculated shock angles and help identify areas of turbulence across the model. An unexpected area of turbulent flow was discovered from schlieren imaging on the chamfered sections of the upper surface of the vehicle, potentially causing rolling turbulent eddy formations located on these chamfered sections.

E. CFD and Wind Tunnel Comparison

To validate CFD against wind tunnel results, two CFD cases were run at wind tunnel conditions to obtain comparable values of surface heat flux. The Mach 7 Ludwieg tube produces laminar flow conditions [33], though the actual vehicle conditions are expected to be almost fully turbulent. To account for this, two cases were run, one with the k-ω turbulence model and one laminar. The geometry is scaled down to mimic the 1/3 scale test article and the input parameters are adjusted to match the wind tunnel test cell conditions as shown in table 4.

Table 4 Physical inputs for wind tunnel CFD

Case	Chemical Kinetics	Thermal Model	M_∞	Re_∞(1/m)	T_∞(K)	T_w(K)	Turbulence
Wind Tunnel (T)	Finite Rate	1T	7.0	5.1x10^6	51.93	298	Wilcox k-ω (2006)
Wind Tunnel (L)	Finite Rate	1T	7.0	5.1x10^6	51.93	298	Laminar

III. Results

A. Shock Formation

The shock formation captured through time-averaged schlieren imaging and a simulated Mach 7 contour from FUN3D are visually compared in Fig. 5. The shock angles are similar between the two data sources, demonstrating agreement and providing confidence in the accuracy of the data collection.

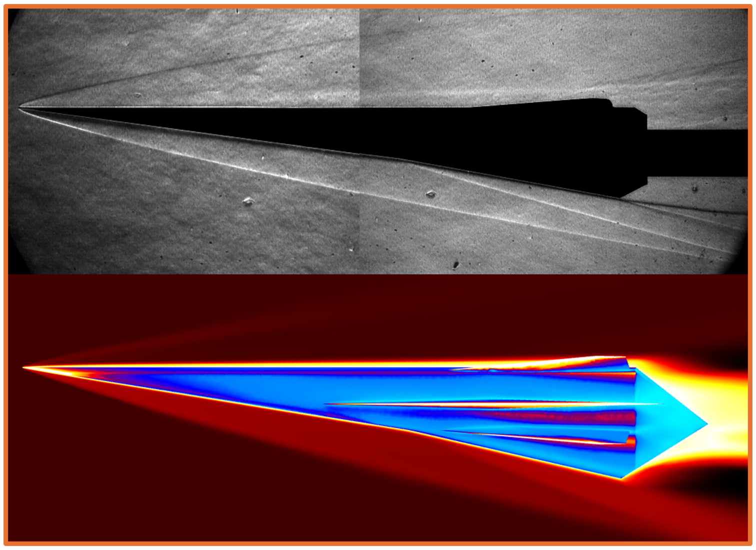

Fig. 5 Shock formation from schlieren imagery (top) and FUN3D (bottom)

B. Surface Heating

Wind tunnel heat flux measurements of the upper and lower vehicle surfaces and a comparison to CFD heat flux data are shown in Fig. 6 and Fig. 7 respectively. While the overall heating distributions match closely, greater deviation was seen near the leading edges, with the FUN3D results reporting far more adverse heat loads in the stagnation regions.

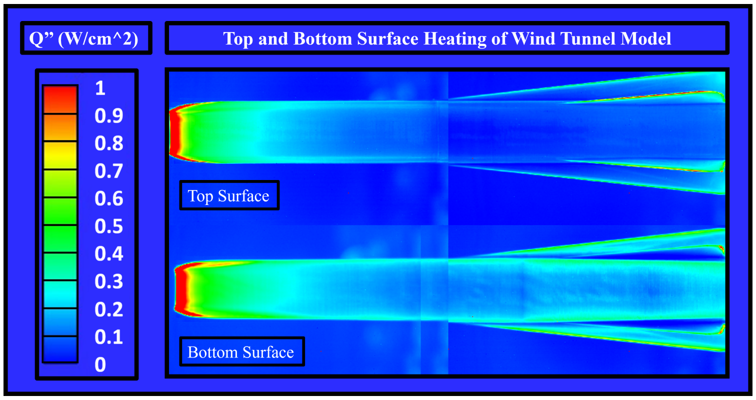

Fig. 6 Surface heating distribution from infrared cameras in wind tunnel

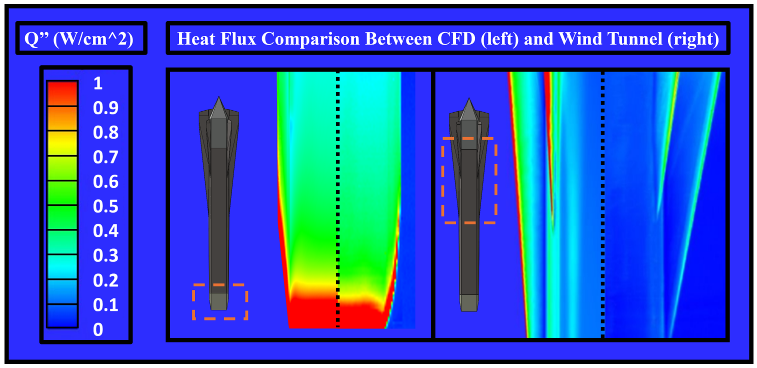

Fig. 7 Wind tunnel vs FUN3D heating comparison, top view, front/rear regions

In Tecplot EX 2025 R1, surface heat flux values were extracted along the symmetry line of the top and bottom surfaces of the vehicle for both the $k - \omega$ and laminar cases. In MATLAB, a similar process was done with the thermal image received from the experiment. The position along the surface x was normalized relative to the total length of the lines sampled. Additionally, the heat flux gradient with respect to the normalized x was found and compared between the three datasets. The wind tunnel results were denoised with a Savitzky–Golay filter to smooth the data [34]. The top and bottom surface heating numbers are compared in Fig. 8 and Fig. 9 respectively.

As previously indicated through the visual comparison of surface heating distribution, the heating values along the top surface of Tachyon demonstrated strong agreement, though the heating near the leading edge varied greatly. The discrepancy in leading edge heating is to be expected, as the 1:3 scale model has very thin leading edges that are difficult to replicate accurately with PLA. In contrast to the top surface, the heat flux values on the bottom surface varied greatly throughout. The spatial heat flux gradients along the sampled lines were very close for the top surface after smoothing the wind tunnel results. For the bottom surface, the gradients were closer for the most part, though extremely steep gradients are present in the FUN3D results around $\frac{x}{x_{ref}} \approx 0.70$. This roughly corresponds to the area where the bottom lifting surface of Tachyon transitions to a steeper inclination, inducing an additional oblique shockwave as shown in Fig. 5. This produces a shock wave/turbulent boundary layer interaction which RANS models notoriously struggle with [35, 36].

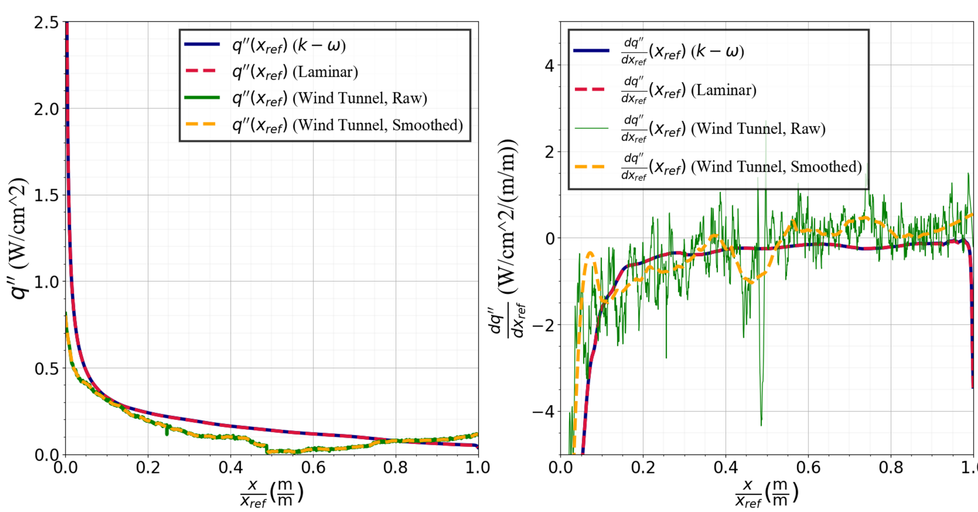

Fig. 8 Comparison of CFD and wind tunnel surface heat flux distribution (left) and gradient (right) along the centerline axis on top of Tachyon

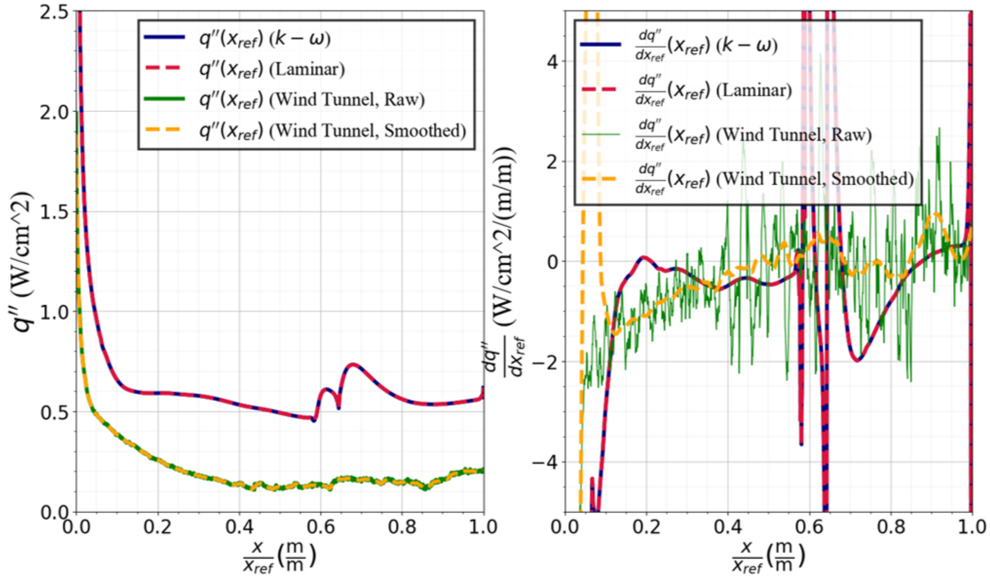

Fig. 9 Comparison of CFD and wind tunnel surface heat flux distribution (left) and gradient (right) along the centerline axis on bottom of Tachyon

IV. Future Data Collection

A. CUBRC LENS Testing

The CUBRC 48-inch Large Energy National Shock tunnel (LENS) in Buffalo, NY, will be used for testing of a full-scale Tachyon model [37]. A similar aerothermal analysis procedure to the method at UTSI will be conducted at LENS, allowing for more heating data to be collected. With a full-scale model, heating characterization near the model's leading edges will be higher quality due to a higher ratio of measurement resolution to the model's surface area. Additionally, at UTSI, the leading edge of the PLA model was damaged over time, with angled edges becoming rounded, as seen in Fig. 6. Testing at LENS with a metal model will limit this concern. LENS also has access to a force balance to measure aerodynamic forces and moments, as well as focusing schlieren imaging, which will allow for validation of the Tachyon CFD and aerodynamic database in addition to studying heating.

B. ARL Gun Launch Testing

At the Army Research Laboratory (ARL), a steel Tachyon model will be launched from a testing gun in a flight test. The model will have similar aerodynamic characteristics to the full design, as the model interior is designed to have a center of mass in the same location as the full design. The model will be launched from a low inclination above the horizon, matching the launch conditions in the design proposal. The model will be tracked downrange during flight by ground-based visual and IR cameras. IR data gathered from tracking ground cameras will be used to validate heating during flight conditions. These data will be used with data from UTSI and LENS tests for further aerothermal analysis and validation of the current aerodynamic database from FUN3D.

V. Conclusion

This paper detailed the computational analysis and experimental validation performed in support of the development of Tachyon, an undergraduate-designed hypersonic glide vehicle. Preliminary shaping and performance assessment were accelerated through CBAERO, while high-fidelity FUN3D simulations provided detailed aerodynamic and heating predictions across the vehicle's expected flight envelope. A Mach 7 ground test campaign at UTSI supplied infrared and schlieren imaging data that enabled direct comparison with CFD results. The strong agreement in shock structure and overall heating distribution demonstrated the reliability of numerical simulation, though notable discrepancies in stagnation-region heating and bottom-surface heat flux magnitude highlighted the limitations of RANS turbulence modeling in heat transfer prediction in areas with complex flow behavior. The results from the analysis provided validation of the aerodynamic performance and thermal survivability of Tachyon, contributing to the success of the project. Upcoming full-scale testing at CUBRC LENS and flight testing at ARL will expand the available dataset, improve resolution near critical geometric features, and further validate aerodynamic and thermal predictions under more representative conditions. Together, these efforts advance the readiness of the Tachyon airframe and contribute to broader hypersonic research and workforce development objectives, particularly at the undergraduate level.

References

[1] Cronk, T. M., "Hypersonics, Counter-Hypersonics Are a Top Priority," U.S. Department of Defense News, Jul. 2020. URL https://www.war.gov/News/News-Stories/Article/Article/2287913/hypersonics-counter-hypersonics-are-a-top-priority/.

[2] Schmisseur, J. D., "Hypersonics into the 21st century: A perspective on AFOSR-sponsored research in aerothermodynamics," *Progress in Aerospace Sciences*, Vol. 72, 2015, pp. 3–16. https://doi.org/https://doi.org/10.1016/j.paerosci.2014.09.009, URL https://www.sciencedirect.com/science/article/pii/S0376042114000980.

[3] Sayler, K. M., "Hypersonic Weapons: Background and Issues for Congress," Congressional Research Service Report R45811, Aug. 2025. URL https://www.congress.gov/crs-product/R45811.

[4] Van Wei, D. M., "Hypersonics: Past, Present, and Potential Future," *Johns Hopkins APL Technical Digest*, Vol. 35, No. 4, 2021.

[5] Khollam, A., "Pentagon Taps Six Vendors for Next-Gen Mach 5+ Hypersonic Missiles," , Feb. 2026. URL https://interestingengineering.com/military/pentagon-jhto-mach-5-hypersonic-missile-contracts, accessed: 2026-02-17.

[6] HigherGov, "Joint Hypersonic Technology Development & Transition," https://www.highergov.com/budget/joint-hypersonic-technology-development-transition-72f9836/, 2025. Accessed: 2026-02-04.

[7] University Consortium for Applied Hypersonics, "About Us," https://hypersonics.tamu.edu/about-us/, 2026. Accessed: 2026-02-04.

[8] University Consortium for Applied Hypersonics, "2025 Undergraduate Hypersonic Flight Design Competition," https://hypersonics.tamu.edu/2025-undergraduate-hypersonic-flight-design-competition/, 2025. Accessed: 2026-02-04.

[9] Leyva, I. A., "The relentless pursuit of hypersonic flight," *Physics Today*, 2017. https://doi.org/10.1063/PT.3.3762, URL https://physicstoday.aip.org/features/the-relentless-pursuit-of-hypersonic-flight.

[10] John D. Anderson, J., *Hypersonic and High Temperature Gas Dynamics*, 4^{th} ed., 2020.

[11] Savino, R., Fumo, M. D. S., Marino, G., and Tului, M., "Aerothermal analysis of an advanced hot structure for hypersonic flight tests," *MRS Proceedings*, Vol. 851, 2004, p. NN11.5. https://doi.org/10.1557/PROC-851-NN11.5.

[12] Sun, J., Zhu, H., Xu, D., and Cai, G., "Aerodynamic Thermal Simulation and Heat Flux Distribution Study of Mechanical Expansion Reentry Vehicle," *Aerospace*, Vol. 10, No. 3, 2023. https://doi.org/10.3390/aerospace10030310, URL https://www.mdpi.com/2226-4310/10/3/310.

[13] van Driest, E. R., "The Problem of Aerodynamic Heating," Los Angeles, California, 1956. Presented at the Aerodynamic Heating: Aerodynamic Aspects Session, National Summer Meeting, IAS, Los Angeles, June 18-21, 1956.

[14] Baurle, R., *Modeling of High Speed Reacting Flows: Established Practices and Future Challenges*, 2012. https://doi.org/10.2514/6.2004-267, URL https://arc.aiaa.org/doi/abs/10.2514/6.2004-267.

[15] Bussing, T. R. A., and Murman, E. M., "Finite-volume method for the calculation of compressible chemically reacting flows," *AIAA Journal*, Vol. 26, No. 9, 1988, pp. 1070–1078. https://doi.org/10.2514/3.10013, URL https://doi.org/10.2514/3.10013.

[16] Sandia National Laboratories, United States National Nuclear Security Administration, and United States Department of Energy, Office of Scientific and Technical Information, "Model Reduction in Reacting Flow," Tech. rep., United States National Nuclear Security Administration, United States, 2014. URL http://www.osti.gov/scitech/biblio/1145216, distributed by the Office of Scientific and Technical Information, U.S. Department of Energy.

[17] Versteeg, H. K., and Malalasekera, W., "An Introduction to Computational Fluid Dynamics: The Finite Volume Method," *An Introduction to Computational Fluid Dynamics: The Finite Volume Method*, Pearson Education, Harlow, England, 2007, Chap. 3, 2^{nd} ed.

[18] Li, A., Wang, T., Chen, J., Xi, G., and Huang, Z., "Application of Uncertainty Quantification of Reynolds-Averaged Navier–Stokes Models in Hypersonic Flow," *AIAA Journal*, Vol. 63, No. 9, 2025, pp. 4001–4009. https://doi.org/10.2514/1.J065602, URL https://doi.org/10.2514/1.J065602.

[19] Murphy, A., and Agarwal, R. K., *Application and Evaluation of the Wray-Agarwal Turbulence Model with Compressibility Corrections in SU2 for RANS Hypersonic Flow Prediction*, 2025. https://doi.org/10.2514/6.2025-3112, URL https://arc.aiaa.org/doi/abs/10.2514/6.2025-3112.

[20] Bose, D., Brown, J. L., Prabhu, D. K., Gnoffo, P., Johnston, C. O., and Hollis, B., "Uncertainty Assessment of Hypersonic Aerothermodynamics Prediction Capability," *42nd AIAA Thermophysics Conference*, American Institute of Aeronautics and Astronautics, Honolulu, HI, USA, 2011. URL https://ntrs.nasa.gov/citations/20110014963, nASA Technical Reports Server (Document ID: 20110014963, Report No. ARC-E-DAA-TN3810).

[21] University of Tennessee Tickle College of Engineering, "UT Hypersonics Team Captures National Title," https://tickle.utk.edu/

news/ut-hypersonics-team-captures-national-title/, 01 2026. Accessed: 2026-02-04.

[22] Center, C.-U. R., "Large Energy National Shock Tunnel (LENS)," https://apps.dtic.mil/sti/citations/ADA338839, 1990. Accession No. ADA338839; Defense Technical Information Center; Accessed: 2026-02-04.

[23] U.S. Army DEVCOM Army Research Laboratory, "DEVCOM Army Research Laboratory," https://arl.devcom.army.mil/, n.d. Accessed: 2026-02-04.

[24] "Configuration-Based Aerodynamics (CBAero) (ARC-15819-1)," https://software.nasa.gov/software/ARC-15819-1, 2025.

[25] *FUN3D Manual*, 2025. URL \url{https://fun3d.larc.nasa.gov/}, accessed: 2025-11-11.

[26] Gragston, M., Davenport, K., Siddiqui, F., Webber, N., Smith, C., Kreth, P., and Schmisseur, J., "Design and Initial Characterization of the UTSI Mach 7 Ludwieg Tube," 2023. https://doi.org/https://doi.org/10.1016/j.applthermaleng.2019.03.126, URL https://arc.aiaa.org/doi/full/10.2514/6.2023-1457.

[27] Wilcox, D. C., "Formulation of the k-ω Turbulence Model Revisited," *AIAA Journal*, Vol. 46, No. 11, 2008, pp. 2823–2838. https://doi.org/10.2514/1.36541.

[28] Yee, H., "Construction of explicit and implicit symmetric TVD schemes and their applications," *Journal of Computational Physics*, Vol. 68, No. 1, 1987, pp. 151–179. https://doi.org/10.1016/0021-9991(87)90049-0.

[29] Menter, F. R., "Two-Equation Eddy-Viscosity Turbulence Models for Engineering Applications," *AIAA Journal*, Vol. 32, No. 8, 1994, pp. 1598–1605. https://doi.org/10.2514/3.12149.

[30] van Leer, B., "Towards the Ultimate Conservative Difference Scheme. II. Monotonicity and Conservation Combined in a Second-Order Scheme," *Journal of Computational Physics*, Vol. 14, No. 4, 1974, pp. 361–370.

[31] van Albada, G. D., van Leer, B., and Roberts, W. W., Jr., "A Comparative Study of Computational Methods in Cosmic Gas Dynamics," *Astronomy and Astrophysics*, Vol. 108, No. 1, 1981, pp. 76–84.

[32] University of Tennessee Space Institute, "Mach 7 Ludwieg Tube," , 2026. Available at https://www.utsi.edu/horizon/facilities/mach-7-ludwieg-tube/, accessed Feb. 4, 2026.

[33] Smith, C. D., Lindorfer, S. A., Edwards, S., Gragston, M., and Mizell, K., *Fast Pressure-Sensitive Paint on Adhesive Film for Improved Test Preparation Efficiency*, 2026. https://doi.org/10.2514/6.2026-0667, URL https://arc.aiaa.org/doi/abs/10.2514/6.2026-0667.

[34] SciPy Developers, *savgol_filter — SciPy v1.17.0 Manual*, SciPy, 2024. URL https://docs.scipy.org/doc/scipy/reference/generated/scipy.signal.savgol_filter.html, accessed: 2026-02-19.

[35] Lindörfer, S. A., Combs, C. S., Kreth, P. A., and Schmisseur, J. D., *Numerical Simulations of a Cylinder-Induced Shock Wave/Boundary Layer Interaction*, 2017. https://doi.org/10.2514/6.2017-0534, URL https://arc.aiaa.org/doi/abs/10.2514/6.2017-0534.

[36] Knight, D. D., and Degrez, G., "Shock Wave Boundary Layer Interactions in High Mach Number Flows: A Critical Survey of Current Numerical Prediction Capabilities," Advisory Report 319, AGARD, Dec. 1998.

[37] Calspan-UB Research Center, "Large Energy National Shock Tunnel (LENS): Description and Capabilities," Tech. Rep. ADA338839, Calspan-UB Research Center, Buffalo, New York, December 1990. Distribution Statement A: Approved for public release; distribution unlimited.